Article

Lithium halide cathodes for Li metal batteries

Jijian Xu, Travis P. Pollard, Chongyin Yang, ..., Anh Ngo, Oleg Borodin, Chunsheng Wang

cswang@umd.edu

Highlights

A family of transition-metal-free cathodes was demonstrated

A generic rule of liquefaction for reversible lithium halide cathodes

Rational non-aqueous electrolyte design to enable lithium halide cathodes
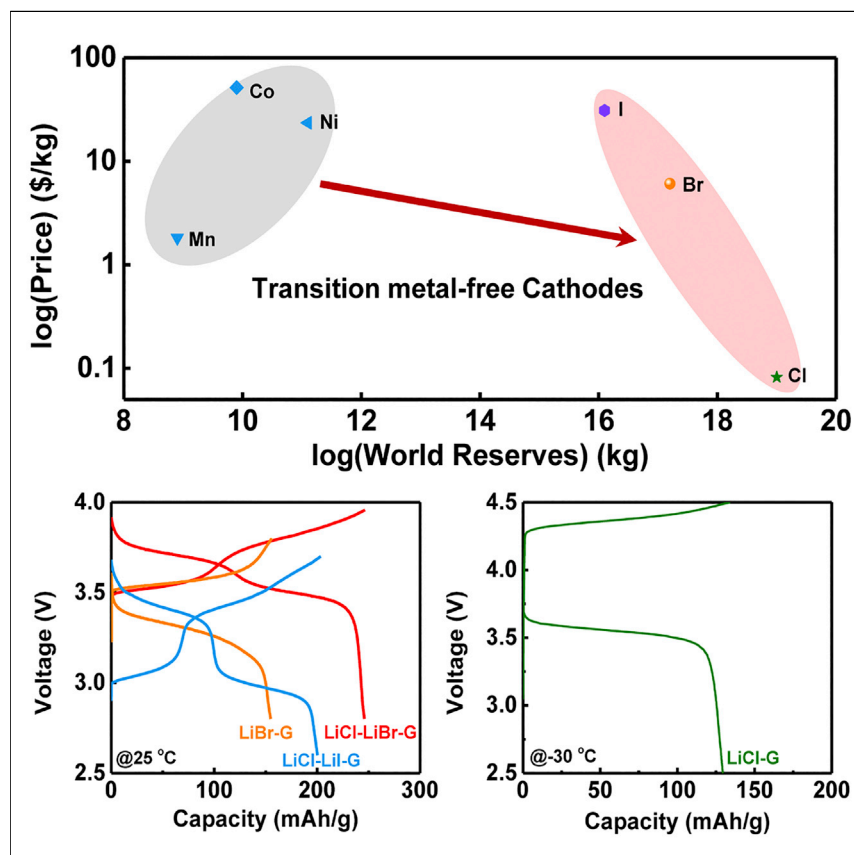
Cathode development is critical to improving energy density and lowering costs of advanced batteries toward green energy transition and net zero emission goals. A family of high-capacity, earth-abundant lithium halide cathodes was developed to reduce the cost and eliminate the use of critical materials such as cobalt and nickel. With the knowledge of the general rule of liquefaction and rational electrolyte design, we open up a previously unexplored space for high-energy, low-cost cathodes.

Joule

CellPress

Article

Lithium halide cathodes for Li metal batteries

Jijian Xu,[1,8] Travis P. Pollard,[2,8] Chongyin Yang,[4,8] Naveen K. Dandu,[6,7] Sha Tan,[3] Jigang Zhou,[5] Jian Wang,[5] Xinzi He,[1] Xiyue Zhang,[1] Ai-Min Li,[1] Enyuan Hu,[3] Xiao-Qing Yang,[3] Anh Ngo,[6,7] Oleg Borodin,[2] and Chunsheng Wang[1,9,*]

SUMMARY

Lithium halide cathodes potentially offer a high energy density at a low cost for rechargeable batteries. However, these cathodes suffer from quick capacity decay in organic electrolytes, and the failure mechanism remains elusive. Here, we report that liquefying the halogen or inter-halogen compounds is a prerequisite for achieving high reversibility for the lithium halide cathodes. The gas or solid halogen can be liquefied by using interhalogen compounds with different electronegativity or changing the temperature. As a proof of concept, reversible LiCl conversion-intercalation chemistry in organic electrolytes is demonstrated by using either redox coupling with less electronegative I/Br to form liquid ICl/BrCl or reducing the temperature to $-30/^\circ$C. The LiCl-LiBr-graphite cathodes in 1.6 M lithium difluoro(oxalato)borate/1.6 M lithium triflate in diglyme electrolytes achieve a high reversible specific capacity of 250 mAh/g at 3.7 V with an energy density comparable to or higher than that of transition metal oxide cathodes at a much lower cost.

INTRODUCTION

The global shift to green energy has triggered an ever-growing demand for advanced batteries that have high energy density and low cost and utilize abundant materials.[1,2] In contrast to the successful advancements of high-capacity anodes (3,860 mAh/g for Li metal or 3,580 mAh/g for Si),[3] conventional layered transition metal oxide cathodes ($LiMO_2$, M = Ni, Co, Mn, etc.) with a low capacity (<220 mAh/g) limit the cell energy density.[4,5] Additionally, the surge in demand for rechargeable batteries coupled with concerns about cobalt and nickel scarcities has led to an increase in materials cost.[6] Cathodes now account for ~51% of total battery cost.[7] It is crucial to explore new battery chemistries with transition-metal-free cathodes such as earth-abundant lithium halides that have a potential to alleviate supply chain challenges and the ever-increasing cost of commercial $LiMO_2$ cathodes.

As a transition-metal-free cathode, Li_2S conversion cathode has a high theoretical gravimetric capacity of 1,166 mAh/g, but the low operation voltage (<2.4 V) requires a high areal capacity (>6 mAh/cm²) for achieving a high energy density.[8,9] Because the halogens (up to I) are more electronegative than S, lithium halides (LiX, X = I, Br, Cl) have high halogen conversion potentials, with 3.0 V for LiI, 3.5 V for LiBr, and 4.0 V for LiCl,[10] making them promising alternatives. However, lithium halides have rarely been investigated as cathodes due to challenges overcoming X_2 reactivity and containment of gaseous products such as Cl_2.[11] Recent strategies for suppressing the loss of Cl_2 include trapping evolved gas in porous C or through chemisorption using iodine or ammonium methyl iodide, though reversibility remains quite

CONTEXT & SCALE

As conventional layered transition metal oxide cathodes approach their theoretical capacity limits (<220 mAh/g) and confront potential cobalt and nickel scarcities, the development of high-capacity and earth-abundant cathodes is key to achieving a global green energy transition. Earth-abundant lithium halides have high theoretical potentials and capacities (LiCl: 632 mAh/g, LiBr: 308 mAh/g, LiI: 190 mAh/g) and thus can provide high energy density.

Herein, a rule of liquefaction is established for the formation of stable graphite intercalated compounds and rationally designed electrolytes to enable lithium halide cathodes with high reversibility. As a proof of concept, reversible LiCl-LiI-graphite, LiCl-LiBr-graphite, and LiBr-graphite cathodes at room temperature, as well as reversible LiCl-graphite cathodes at -30°C, were demonstrated. These insights pave the way for the development of new cathodes and their electrolyte designs.

CellPress

Joule
Article

low.[12–14] The most effective method to date is the intercalation of interhalogen species (BrCl) into graphite interlayers from a biphasic highly concentrated aqueous electrolyte.[15] The formation of Cl-containing interhalogen species promotes liquefaction rather than gassing as the boiling point increases from $-34°C$ (Cl_2) to $5°C$ (BrCl) or $98°C$ (ICl). Unfortunately, the high cathodic potential of 1.9 V for water-in-salt electrolytes limits cell voltage and energy density.

The organic electrolyte design is another critical challenge for lithium halide cathodes because the halogen X_2 species at charged states can react with most of the organic electrolytes. Glymes are an excellent alternative for extending cathodic stability, though a low anodic stability (<4 V) hinders their application to Cl-containing lithium halide cathodes.[16–18] One approach to enhance the high-voltage stability of the electrolytes is to add more salts since the high-concentration electrolytes can push the charge cutoff voltage up to 4.5 V,[19,20] due to the formation of a robust cathode-electrolyte interphase (CEI).[21,22] CEI can effectively isolate the active materials from electrolytes to avoid active material dissolution and electrolyte degradation.[23,24]

Herein, we developed a quasi-ionic liquid electrolyte (1.6 M lithium difluoro[oxalate]borate [LiDFOB]/1.6 M lithium triflate [LiOTF] salts in diglyme [G2] solvent) with almost no free solvent, which enables both Li anode and lithium halide cathodes to achieve a high energy density and long cycle life. Halogens are liquefied either by forming interhalogen species or reducing cell operation temperature and have low solubility in the quasi-ionic liquid electrolyte. Room-temperature LiCl-LiI-graphite, LiCl-LiBr-graphite, and LiBr-graphite cathodes as well as reversible LiCl-graphite cathodes at $-30°C$ were used to validate the design principle of liquefied (inter)halogen intercalation into graphite. Density functional theory (DFT) calculations and experimental analysis confirmed that Br-activated LiDFOB ring-open polymerization formed a robust CEI on lithium halide cathodes, which enhanced anodic stability to 4.8 V. The CEI further reduces solubility of the halogens in the electrolyte and eliminates undesired shuttling effects. As a demonstration, LiCl-LiBr-graphite||Li (20 μm) pouch cell achieved 2.5 mAh cm^{-2} with Coulombic efficiency (CE) of 99.5% for 200 cycles. Moreover, LiCl-LiBr-graphite cathodes can provide 62% of the room-temperature capacity at $-30°C$.

RESULTS AND DISCUSSION

Mechanism of lithium halide cathodes

The charge and discharge behavior of lithium halides||Li cells was examined: on charge, the Li cation in cathodes is transported through the electrolyte and electrochemically deposited on Li anode while the halide anion is oxidized into halogen and intercalated into graphite. The reverse reaction occurs on discharge. The lithium halide has poor solubility in quasi-ionic liquid electrolyte, which enhances reversibility of the conversion-intercalation reaction and minimizes shuttle effects. The formation of interphase screens lithium halides from the electrolyte, further reducing solubility of the lithium halides in the electrolyte and enhancing reversibility of the cathode reaction. Figure 1A shows the liquid temperature of halogens and interhalogens versus their redox potential. The graphite intercalation potentials of halogens depend on the solvation structure of the electrolytes. At room temperature, the redox potentials range from 3.0 to 4.5 V, with (inter)halogen solids (I_2, IBr) at the low end of this range, (inter)halogen liquids (ICl, Br_2, and BrCl) at intermediate potentials, and gaseous Cl_2 at the highest potential. Unfortunately, formation of gaseous Cl_2 with no intercalation compromises the reversibility of LiCl-graphite

[1]Department of Chemical and Biomolecular Engineering, University of Maryland, College Park, MD 20742, USA

[2]Battery Science Branch, Army Research Directorate, US DEVCOM Army Research Laboratory, Adelphi, MD 20783, USA

[3]Chemistry Division, Brookhaven National Laboratory, Upton, NY 11973, USA

[4]Department of Physics and Atmosphere Science, Dalhousie University, Halifax, NS B3H 4R2, Canada

[5]Canadian Light Source Inc., University of Saskatchewan, Saskatoon, SK S7N 2V3, Canada

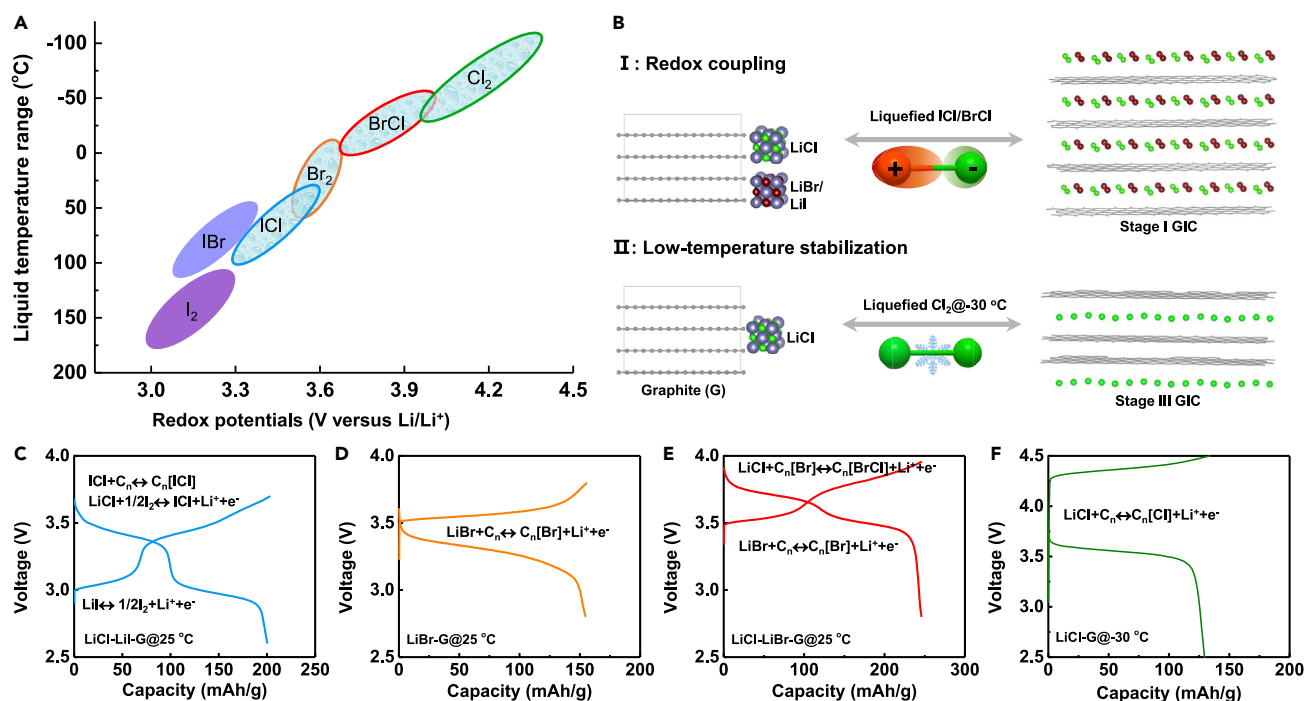[6]Materials Science Division, Argonne National Laboratory, Lemont, IL 60439, USA

[7]Chemical Engineering Department, University of Illinois-Chicago, Chicago, IL 60607, USA

[8]These authors contributed equally

[9]Lead contact

*Correspondence: cswang@umd.edu

https://doi.org/10.1016/j.joule.2022.11.002

Joule
Article

CellPress

Figure 1. Chemistry of lithium halide conversion-intercalation cathodes

(A) Liquid temperature range and graphite intercalation potential of halogens and interhalogens.

(B) Liquefying Cl by forming ICl and BrCl interhalogens or reducing the temperature to −30°C to form stable graphite intercalated compounds (GICs).

(C–F) Potential profiles for halogen intercalation/deintercalation into graphite process at the third cycle of (C) LiCl-LiI-graphite under 25°C, (D) LiBr-graphite under 25°C, (E) LiCl-LiBr-graphite under 25°C, and (F) LiCl-graphite under −30°C.

cathodes during charging (Figure S1). Although dropping the operating temperature to −30°C can liquefy the Cl_2 gas into a liquid, allowing reversible Cl_2 intercalation into graphite cathodes (Figure 1F), the extremely low operation temperature limits the application of LiCl-graphite cathodes. Br_2 is in a liquid state at room temperature, but LiBr-graphite cathode has a low energy density (see Figure 1D, low potential of 3.5 V and low capacity of 150 mAh/g) because Br has a low affinity to graphite and can only form stage-II graphite intercalation compounds. In contrast, I_2 is solid at 25°C, which cannot intercalate into graphite at room temperature.[25] Figure 1A suggests that adding less electronegative Br or I can convert gaseous Cl_2 into liquid BrCl and ICl interhalogens compounds at room temperature, respectively. Liquefaction of the (inter)halogen species enables reversible intercalation/deintercalation in/from graphite (Figure 1B). The LiCl-LiI-graphite (Figure 1C) and LiCl-LiBr-graphite (Figure 1E) cathodes show similar two-stage reactions, but with slightly different reaction steps. As for LiCl-LiI-graphite cathodes, iodine and Cl are simultaneously inserted into graphite because solid iodine alone cannot be inserted into graphite. LiCl and LiI are converted into liquid ICl and then insert into the graphite upon charging (Figure 1C). As for LiCl-LiBr-graphite cathodes, the Br intercalates into graphite first, followed by the Cl intercalation forming stage I $C_n[BrCl]$ (Figure 1E). The average reaction potential of LiCl-LiBr-graphite cathodes in non-aqueous electrolytes is about 3.7 V, which is lower than that (4.2 V) in aqueous electrolytes.[15] The galvanostatic intermittent titration (GITT) analysis of LiCl-LiBr-graphite cathodes in the quasi-ionic liquid electrolyte (Figure S2A) demonstrated that the intercalation/deintercalation potential drop in the organic electrolyte is attributed to thermodynamic not kinetics. DFT calculations attribute the step-increase in potential versus capacity to consecutive intercalation of Br and Cl from

stages VIII, VI, IV (Br), stage-II (Br) to stage I (BrCl) (Figure S2B). Intercalation is accompanied by volume changes in the cathode from 52% (stage II, Br only) to 105% (stage I, BrCl) with a carbon-halogen-carbon interlayer separation of ~6.85 Å. The lowest energy intercalate structures for each stage/composition are shown in Figure S2C (stages IV+ assume the stage-II intercalate structure is preserved, just adding additional empty galleries). The potential shift in the G2 based electrolyte versus previously investigated aqueous electrolytes[15] is attributed to differences in desolvation energies. LiCl-LiBr in the bisphasic water-in-salt electrolyte is either added as a monohydrate salt or absorbs water from the water-in-salt phase, resulting in a larger desolvation contribution to the potential (we computed desolvation energies from Li-X contact ion pairs). LiCl-LiBr are known to be more aggregating in monoglyme, and the low solubility observed here,[26] especially after formation of the CEI, results in a lower desolvation energy per formula unit (computed from clusters of $(LiX)_{2,4}$). The similarity between measured experimental intercalation potential from GITT (Figure S2A) and calculated intercalation potential from DFT confirmed the critical role of electrolyte desolvation energies in intercalation potential.

In summary, solid I_2 and gaseous Cl_2 (Figure S1) alone cannot intercalate into graphite,[13,14] but the liquid ICl interhalogen can reversibly co-intercalate into graphite (Figure 1C). In addition, liquid Br_2 can intercalate into graphite and confine Cl into liquid BrCl owing to strong confinement in graphite interlayers,[27] making BrCl co-intercalation highly reversible (Figure 1E). Liquefying Cl_2 gas at $-30°C$ also makes Cl_2-graphite intercalation reaction highly reversible (Figure 1F). Therefore, the liquefaction of halogens is a prerequisite to forming stable graphite intercalation compounds.

Design of non-aqueous electrolyte

To support lithium halides||Li cells, the non-aqueous electrolyte should be stable with halogen anion at high voltages as well as have a low solubility to lithium halides and halogens. The experience with Li-O_2 battery development suggests that glyme solvents monoglyme (G1), G2, triglyme (G3), and tetraglyme (G4) are stable with lithium halide cathodes.[28] In addition, glymes such as G2, G3, and G4 can form one-to-one complexes with some lithium salts (such as LiOTF), exhibiting quasi-ionic liquid behaviors at high-salt concentrations,[29,30] which can enhance the anodic stability window and reduce the solubility to halogens and halides. Therefore, we selected high-concentration LiOTF/glyme quasi-ionic electrolytes with an ether oxygen:cation ratio of 5.2:1 for initial screening. Br_2 was selected among the halogens X_2 (X = I, Br, Cl) to evaluate the LiOTF/glyme quasi-ionic electrolytes because Br_2 is easier to handle in the liquid state.

The Br_2 solubility in different quasi-ionic liquid electrolytes is analyzed using the ultraviolet-visible (UV-vis) spectra (Figure 2A) after adding Br_2 to the LiOTF/glyme electrolytes and resting for 24 h. The absorption peak at 408 nm is from Br_2, as reported in previous literature.[31] The peak intensity decreases in the order of G1 > G3 > G2 ≈ G4, demonstrating that Br_2 has a lower solubility in G2 electrolytes. Since G2 also has a lower viscosity, LiOTF-G2 was selected as a quasi-ionic electrolyte for further study. LiOTF-G2 quasi-ionic liquid electrolytes are highly aggregating, leaving trace amounts of free solvent for dissolving liquid Br_2. Consequently, the liquid Br_2 is visually phase-separated from the LiOTF-G2 quasi-ionic liquid electrolyte, as demonstrated by the insert photo in Figure 2A. The bottom layer with brownish-red color is liquid Br_2, whereas the upper layer is the LiOTF-G2 electrolyte. Analysis of *ab initio* molecular dynamics (AIMDs) simulations indicates halide
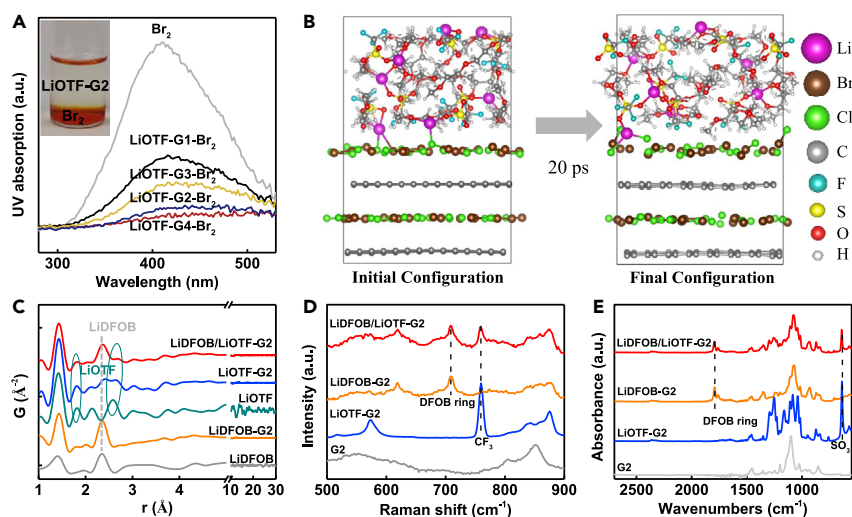
Figure 2. Solvation structure and properties of the designed electrolytes

(A) UV-vis spectra of G1, G2, G3, and G4-based electrolytes after adding Br_2 into electrolytes and rest for 24 h. Insert: photo of LiOTF-G2 electrolyte in contact with liquid Br_2, demonstrating liquid Br_2 is phase-separated from the quasi-ionic liquid electrolyte.

(B) A snapshot of initial and final configurations before and after the AIMD simulations at 20 ps for the LiOTF-G2 electrolyte on the cathode, indicating Br/Cl was not dissolved in the electrolyte.

(C) PDF data of designed electrolytes and single lithium salts.

(D and E) Raman spectra (D) and ATR spectra (E) of different electrolytes and bare G2 solvent for comparison.

solubility is low, whereas some Br/Cl still can diffuse into the electrolyte at the simulation timescale (Figure 2B; Video S1).

Further decrease of Br_2 dissolution into electrolyte during battery cycling is achieved via formation of CEI that serves as an additional barrier for (inter)halogen diffusion between the cathode surface and electrolyte. A LiDFOB salt was chosen as a robust and effective CEI former.[32] Figure S3 shows the oxidation stability of LiDFOB-G2 and LiDFOB/LiOTF-G2 electrolytes. LiDFOB starts to oxidize at 3.9 V (red line) in LiDFOB-G2 and passivate the electrode. The formation of CEI from the decomposition of LiDFOB in LiDFOB/LiOTF-G2 electrolytes largely extends the oxidation stability potential to 4.8 V. The AIMD simulation result of LiDFOB/LiOTF-G2 is presented in Video S2. The dual-salt electrolyte shows synergistic effects in which the already low solubility of Br_2 in LiOTF-G2 is further reduced by the CEI formed from decomposition of LiDFOB.

The pair distribution function (PDF) is a powerful tool to probe the local structure of concentrated electrolytes.[33] As shown in Figure 2C, LiDFOB and LiOTF pure salts possess longer-range ordering (>10 Å) because of their high crystallinity. The primary peak at ~1.4 Å is attributed to short bonds inside lithium salts such as C=O, C–O, B–F, B–O, C–F, etc.[34] In the LiDFOB-G2 electrolyte, LiDFOB salt shares almost the same PDF peaks confirming the quasi-ionic liquid nature of the electrolytes. Similarly, LiOTF-G2 electrolytes also have similar PDF peaks with LiOTF salt. Importantly, dual-salt electrolyte (LiDFOB/LiOTF-G2) inherits the solvation structure from the single salt systems, as outlined by the dark-cyan circles and gray dash line features.

The Raman and attenuated total reflectance (ATR) spectra also confirmed that the dual-salt electrolyte (LiDFOB/LiOTF-G2) inherits the quasi-ionic liquid structure
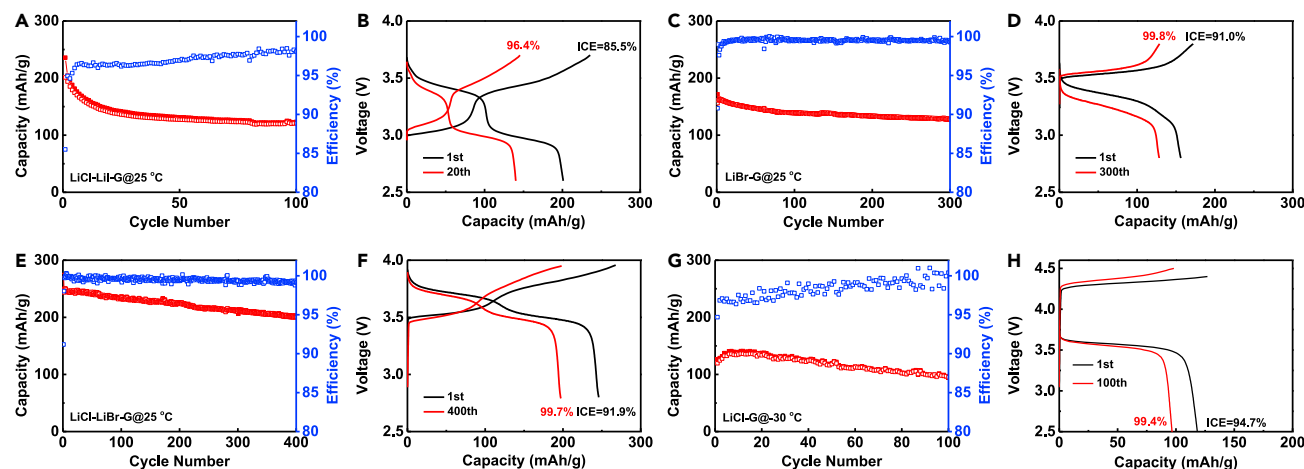
Figure 3. Electrochemical performance of 2.5 mAh/cm² lithium halides‖Li cells with LiDFOB/LiOTF-G2 electrolytes
Cycling performance and corresponding voltage curves of (A and B) LiCl-LiI-graphite, (C and D) LiBr-graphite, (E and F) LiCl-LiBr-graphite cathodes using LiDFOB/LiOTF-G2 electrolyte at 0.3 C under 25°C, (G) cycling performance of LiCl-graphite cathodes at 0.1 C under −30°C, and (H) corresponding voltage curves.

from single salt (LiDFOB-G2 and LiOTF-G2) systems (Figures 2D and 2E). The characteristic peaks of both LiDFOB and LiOTF are observed at the same position in the Raman spectrum of LiDFOB/LiOTF-G2 electrolyte. The strong peak observed at 709 cm^{-1} in both LiDFOB-G2 and LiDFOB/LiOTF-G2 corresponds to the solvated LiDFOB ring breathing vibration.[35] The peak located at 761 cm^{-1} in LiOTF-G2 and LiDFOB/LiOTF-G2 are attributed to aggregates of LiOTF.[34,36] In the ATR spectrum in Figure 2E, the 637 cm^{-1} band of SO_3 (LiOTF salt) symmetric deformation in LiOTF-G2 electrolyte and the 1,795 cm^{-1} band of DFOB ring oscillation in LiDFOB-G2 electrolyte remain unshifted in LiDFOB/LiOTF-G2 electrolyte.

Electrochemical performance of lithium halide cathodes

On the basis of design principles of lithium halide cathodes and electrolytes, all the liquefied lithium halide cathodes (LiCl-graphite at −30°C; LiCl-LiI-graphite, LiBr-graphite, and LiCl-LiBr-graphite) were evaluated in coin cells using LiDFOB/LiOTF-G2 electrolyte and Li anode (Data S1). As shown in Figure 3A, the LiCl-LiI-graphite‖Li cells can be reversibly charged/discharged achieving an initial capacity of 200 mAh/g with a CE of 86%. However, capacity gradually reduced to 120 mAh/g after 100 cycles due to low CE at 0.3 C (1 C = 250 mA/g). According to the first charging profile in Figure 3B, two well-defined plateaus at around 3.0 and 3.5 V can be identified as the redox stage of I$^-$/I$_2$ (I$_2$Cl$^-$) and ICl conversion reactions.[37] A significant capacity decay in the first 20 cycles (Figures 3A and R1) is mainly attributed to the capacity decay at the low-voltage plateau as demonstrated in the charging process (Figure 3B). The solid I$_2$ generated through the first stage reaction cannot insert into graphite by itself contributing to capacity fade. I$_2$ without forming liquid ICl may dissolve into the electrolyte, forming I$_2$Cl$^-$ and diffusing to the anode, resulting in side reactions. Unsurprisingly, the CE of LiCl-LiI-graphite cathode is well below 99%.
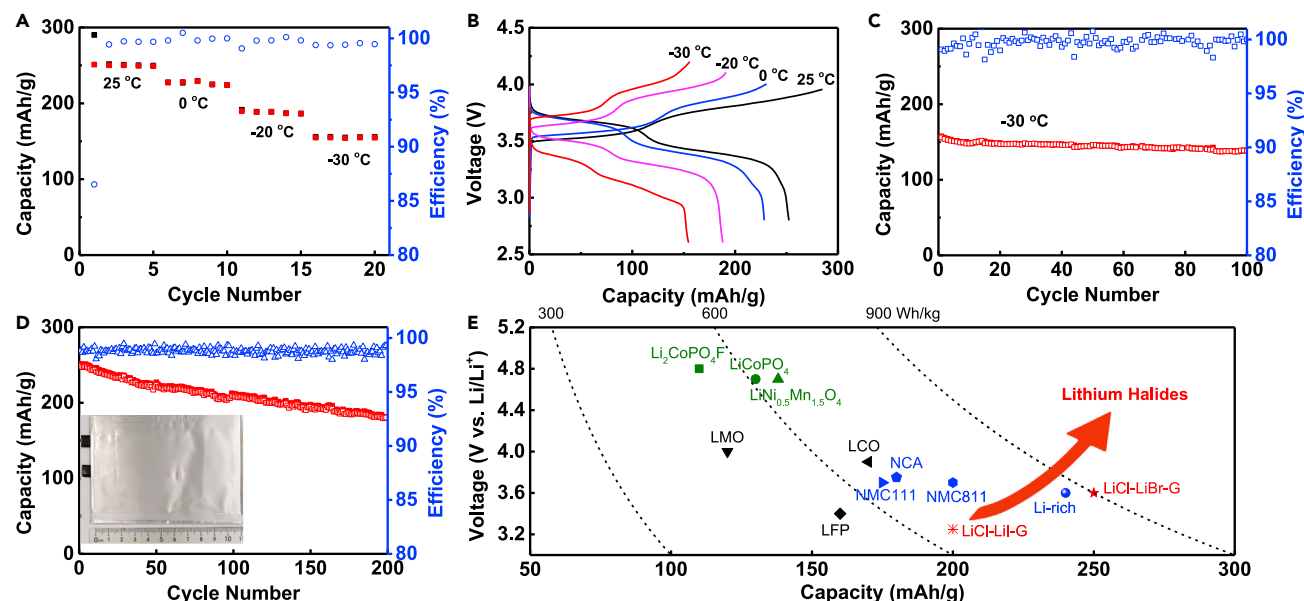
The cycling performance of the LiBr-graphite cathode is greatly improved using the same LiDFOB/LiOTF-G2 electrolytes with 82% of capacity retention after 300 cycles (Figures 3C and 3D). The high cycling stability is because (1) the liquid Br$_2$ generated by conversion reaction in LiBr-graphite cathode is capable of inserting into graphite, and (2) the designed electrolyte is phase-separated from liquid Br$_2$.

Joule
Article

 CellPress

A high reversible capacity of 250 mAh/g with a high initial CE of 91.9% is obtained for LiCl-LiBr-graphite cathode. The crucial BrCl intermediate enabled LiCl-LiBr-graphite cathode to retain 80% of its initial capacity after 400 cycles (Figure 3E). First, the formation of BrCl intermediate converts gaseous Cl_2 into liquid BrCl, making it reversible at room temperature. Second, BrCl intermediate also accelerates the intercalation kinetics. Voltage curves are presented in Figure 3F, for the first and 400th cycles, highlighting the typical two-stage reactions corresponding to the oxidation of Br^- (~3.6 V) and Cl^- (~3.8 V) and their subsequent intercalation into the graphitic structure. The graphite used for the LiCl-LiBr-graphite cathode was surface-fluorinated to form LiF-rich CEI, which improves cycling stability. After the surface fluorination process,[38] the surface layer of graphite is highly fluorinated while bulk graphite retains the graphitic structure, which is beneficial for the formation of a LiF-rich CEI. To verify the important role of CEI, artificial CEI on the LiCl-LiBr-graphite cathode via atomic layer deposition of 4-nm Al_2O_3 has been examined (Figure S4). Figure S5 shows the scanning electron microscope (SEM) image and energy-dispersive X-ray spectroscopy (EDS) result of cycled Li with no observable Br or Cl signal, indicating that the halogens were successfully confined within cathode owing to the formation of the graphite intercalation compounds, minimal dissolution in electrolytes due to the choice of solvate-ionic liquid-like electrolyte, and robust CEI formation. Figure S6 shows the rate performance of LiCl-LiBr-graphite cathode with capacities of 189.3 (78%), 133.9 (55%), and 103.6 (43%) mAh/g at 1 C (2.5 mA/cm^2), 2 C (5.0 mA/cm^2), and 3 C (7.5 mA/cm^2), respectively. Since liquid halogen intercalation into graphite can be very fast (Br diffusion coefficient in graphite, $D = 4.2 \times 10^{-8}$ cm^2/s),[39] the rate-limiting step may be the charge transfer and diffusion/dissociation of Br^- and Cl^- from solid salts. As discussed previously, this trade-off may be beneficial for lowering the oxidation and intercalation potential of BrCl.

Alternatively, a reversible LiCl-graphite cathode was achieved under −30°C (Figures 3G and 3H). The gaseous Cl_2 will easily evaporate from the graphite surface rather than intercalate into the graphite (Figure S1) until the temperature is below the liquefaction temperature (Figures 3G and 3H). This is consistent with the reported result that Cl_2 does not intercalate above −20°C.[40] The LiCl-graphite cathode shows high cycling stability (Figure 3G) with a large charge/discharge overpotentials (Figure 3H). Summarizing the findings from the electrochemical performance of lithium halide cathodes, it is evident that the liquefaction of the (inter) halogen is crucial to the reversibility of the lithium halide cathode.

Since LiCl-LiBr-graphite cathodes have a high intercalation potential (3.7 V) and large capacity (250 mAh/g) and long cycle life, the LiCl-LiBr-graphite was selected as a model liquefied interhalogen-graphite cathode for further study. According to the proposed liquefying halogens rule, the LiCl-LiBr-graphite cathode is expected to have high performance at low temperatures. Differential scanning calorimetry (DSC) characterization suggests that LiDFOB/LiOTF-G2 electrolyte is capable of supporting LiCl-LiBr-graphite||Li cells at low temperature with sufficient ionic conductivity (0.03 mS/cm at −30°C, Figure S7). LiCl-LiBr-graphite||Li cells were then charged/discharged at 0.1 C rate under various temperatures (Figures 4A and 4B). The capacity of LiCl-LiBr-graphite cathodes retains 225.0 (90%), 186.6 (75%), 155.5 (62%) mAh/g when they are cycled at 0°C, −20°C, −30°C, respectively. Representative voltage curves at different temperatures are shown in Figure 4B. Figure 4C shows the impressive cycling performance of LiCl-LiBr-graphite cathodes at 0.1 C at −30°C, retaining 90% after 100 cycles with an average CE of 99.9%.

Figure 4. Electrochemical performance of LiCl-LiBr-graphite||Li cell

(A and B) (A) Cycling performance of LiCl-LiBr-graphite cathode at 0.1 C under different temperatures (25°C, 0°C, −20°C, and −30°C), (B) corresponding voltage profiles.

(C) Long cycling performance at 0.1 C under −30°C.

(D) Cycling performance of LiCl-LiBr-graphite (2.5 mAh/cm^2)||Li (20 μm) pouch cells at 25°C at 0.3 C, insert: photo image of the assembled pouch cell.

(E) Comparison of relevant Li-ion batteries employing different cathodes.

Figures 4D and R2 show the cycling performance of LiCl-LiBr-graphite||Li (20 μm) pouch cells at 25°C in 1.5 M LiDFOB/1.5 M LiOTF/0.2 M LiNO$_3$-G2 electrolyte while preserving the Li$^+$:G2 molar ratio of 4:7. The inclusion of LiNO$_3$ additive combats the formation of Li dendrites and increases the Li plating/stripping CE to a high value of 99.2% at a current of 0.5 mA/cm^2 and a capacity of 1.0 mAh/cm^2 (Figure S8).[41] Figure S9 shows the typical SEM image of the LiCl-LiBr-graphite electrode with a thickness of 45 μm. The related element mappings indicate the uniform dispersion of Br and Cl elements. A high discharge capacity of 242 mAh/g (based on cathode mass) is obtained at 0.3 C. Overall, the cycling performance is stable, retaining 77% after 200 cycles. The fully charged LiBr-LiCl-graphite||Li pouch cell also shows a low self-discharge rate (Figure S10A). At a higher current density of 2.5 mA/cm^2 (1 C), the LiCl-LiBr-graphite (2.5 mAh/cm^2)||Li (20 μm) pouch cells also can achieve stable cycling (Figure S10B). The energy density of the LiCl-LiBr-graphite (2.5 mAh/cm^2)||Li (20 μm) pouch cell is calculated to be as high as 770 Wh kg^{-1} (of total electrode mass including both LiCl-LiBr-graphite and excess lithium).

The energy density of LiCl-LiBr-graphite cathodes was compared with those of commercially available transition metal oxide cathodes (Figure 4E). Despite the similar voltage compared with LiMO$_2$-type materials (3.6 versus 3.7 V), the substantially higher specific capacity of the LiCl-LiBr-graphite cathodes (250 versus 200 mAh/g for NMC811) is related to the higher specific energy. As an example, LiCl-LiBr-graphite cathodes possess such merits as high energy, low cost, and high availability. Additionally, the reversible Cl chemistry achieved at low temperature opens new directions toward high energy density lithium halide cathodes.[42]

Characterization of the interfacial chemistry

Ex situ soft X-ray absorption spectroscopy (XAS) was applied to reveal the BrCl intercalation process of LiCl-LiBr-graphite cathodes at different states of charging (SOCs).
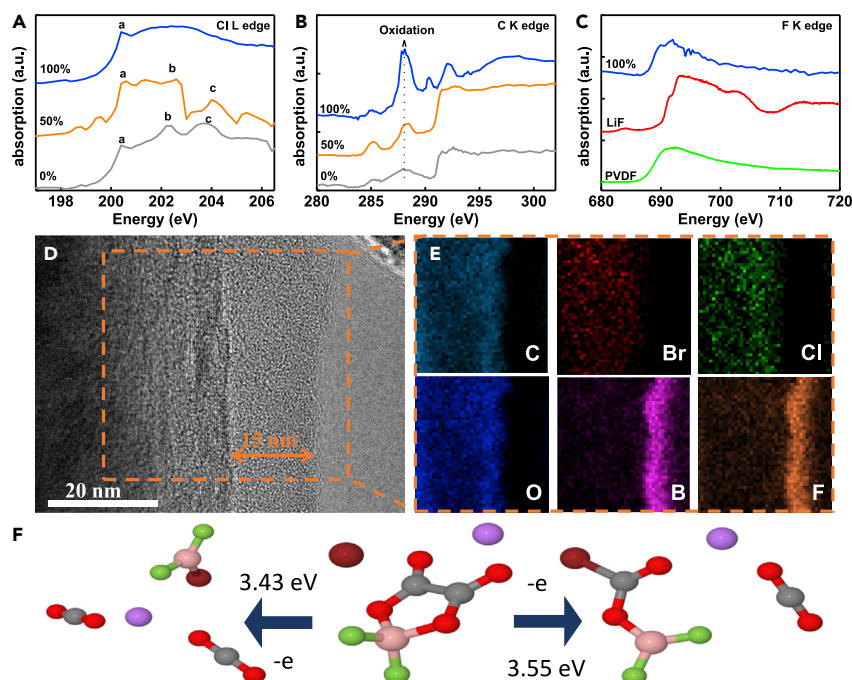
Figure 5. Structure change of LiCl-LiBr-graphite cathodes during charge/discharge cycles and interphase characterization

(A–C) XAS spectra involving the (A) Cl L-edge, (B) C K-edge of LiCl-LiBr-graphite cathodes acquired *ex situ* during the 10th charging process. (C) F K-edge of 10th fully charged LiCl-LiBr-graphite cathodes.

(D and E) Typical (D) HRTEM image of fully charged LiCl-LiBr-graphite cathodes and corresponding (E) EELS elemental mapping of C, Br, Cl, O, B, and F in the selected region.

(F) Schematic of Br-mediated DFOB⁻ open-ring reaction pathways, forming robust CEI. The color scheme: C, gray; O, red; B, pink; F, green; lithium ions, purple; Br, dark red.

Figure 5A shows the Cl L-edge spectra, the peak positions for 0% SOC agree very closely with the reported values of LiCl, indicating Cl in a crystalline state.[43] Upon charging, the edge and peak centers gradually shift to lower energy along with the disappearance of the peak splitting around 202 eV. The disappearance of 202 eV peak splitting is a sign of the formation of atomic BrCl in the fully charged sample. As for the C K-edge in Figure 5B, the peak centered at 288 eV gradually increases along with charging, inferring the possible oxidation of graphite or electron shift away from C to halides. The disappearance of 292 eV splitting indicates a distortion in the graphite structure.[44] The F K-edge spectra in Figure 5C verify the formation of LiF-rich CEI. The pre-edge (~689 eV) and main edge (~692 eV) are raised by C–F bonding in PVDF and LiF in CEI.[45] The different F-related components can also be seen in F spectroptychography difference maps at 689.8 and 692.3 eV, as shown in Figure S11.

Since the CEI plays a critical role in the electrochemical performance of LiCl-LiBr-graphite cathodes, the CEI on cycled LiCl-LiBr-graphite cathodes was also analyzed. Under high-resolution transmission electron microscopy (HRTEM), a uniform and thin CEI of around 15-nm thickness is generated on the LiCl-LiBr-graphite cathodes after 10 cycles in the quasi-ionic liquid electrolyte (Figure 5D). To identify the chemical composition of the CEI on cycled LiCl-LiBr-graphite cathodes, the element mappings of electron-loss spectroscopy (EELS) were employed. Figure 5E shows the distribution of C, Br, Cl, O, B, and F elements, in which B and F elements display brighter contrast in the region of CEI. The time-of-flight secondary ion mass spectrometry (ToF-SIMS) spectra, as well as X-ray

photoelectron spectroscopy (XPS) with an Ar^+ sputtering depth profiling were further used to characterize the formed CEI. In Figure S12A, C_2^-, Cl^-, Br^- second ions are caused by the intrinsic cathode materials while O^-, BO^-, BF_2^- species are derived from DFOB anion during the formation of CEI. Figure S12B shows the edge surface of the crater sputtered by Ga^+ ions with a depth of 1.3 μm. According to the concentration depth profiles (Figure S12C), F^- concentrations decrease quickly with etching, indicating the formation of LiF-rich CEI. XPS results of the cycled LiCl-LiBr-graphite electrodes in Figure S13 agree well with ToF-SIMS results, demonstrating that the CEI is mainly composed of LiF and B-F species derived from LiDFOB salt.

The formation mechanism for CEI from the decomposition of LiDFOB was proposed. As shown in Figure 5F, the B in the LiDFOB salt and the atomic Br center of the cathode surface are bound by a nucleophilic substitution reaction. Subsequent ring-opening polymerization of the DFOB effectively passivates the cathode surface which inhibits the direct contact of the electrolyte solvent and the reactive cathode materials. All experimentally observed CEI components and distributions are in good agreement with this formation mechanism. Undoubtedly, the design of electrolyte and CEI formation play a critical role in stabilizing the aggressive lithium halide cathodes.

Conclusions

Adoption of a quasi-ionic liquid electrolyte and halogen liquefaction enables the reversible and stable operation of lithium halide cathodes in Li metal batteries. The halide salts and oxidation products have low solubility in LiDFOB-LiOTF/G2 quasi-ionic liquid electrolyte and can form LiF-rich CEI. The CEI further inhibits the loss of (inter)halogen species and significantly enhances the cycling stability of halide-graphite cathodes. Most importantly, the liquefaction of gas halogens by other less electronegative halogens is a prerequisite to forming high-voltage graphite intercalation cathodes. Using LiCl-LiBr-graphite as an example, a LiCl-LiBr-graphite cathode||Li (20 μm) pouch cell can achieve an average CE of 99.5% for 200 cycles at a practical loading (2.5 mAh cm^{-2}). Notably, LiCl-LiBr-graphite cathodes can deliver 62% of the room-temperature capacity even at −30°C. The lithium halide cathodes offer unprecedented opportunities for high energy density transition-metal-free cathodes.

EXPERIMENTAL PROCEDURES

Resource availability

Lead contact

Further information and requests for resources and materials should be directed to and will be fulfilled by the lead contact, Chunsheng Wang (cswang@umd.edu).

Materials availability

This study did not generate new unique materials.

Data and code availability

The data supporting the findings of this study are available within the main text and the supplemental information. More detailed data and the code for simulation can be made available upon request to the corresponding author.

Full details of all experiments and simulations are provided in supplemental information.

SUPPLEMENTAL INFORMATION

Supplemental information can be found online at https://doi.org/10.1016/j.joule.2022.11.002.

Joule
Article

CellPress

ACKNOWLEDGMENTS

AUTHOR CONTRIBUTIONS

J.X. and C.W. conceived the idea for the project and wrote the manuscript. T.P.P. and O.B. conducted DFT calculations of intercalation voltage profiles and decomposition potentials. N.K.D. and A.N. carried out *ab initio* molecular dynamics simulations. S.T., E.H., and X.-Q.Y. conducted X-ray absorption experiments. J.Z. and J.W. carried out soft X-ray absorption spectroscopy. C.Y., X.H., X.Z., and A.-M.L. assisted in electrochemical cell tests. All the authors discussed the results and analyzed the data.

DECLARATION OF INTERESTS

The authors declare no competing interests.

REFERENCES

1. Goodenough, J.B., and Kim, Y. (2010). Challenges for rechargeable Li batteries. Chem. Mater. *22*, 587–603. https://doi.org/10.1021/cm901452z.

2. Winter, M., Barnett, B., and Xu, K. (2018). Before Li ion batteries. Chem. Rev. *118*, 11433–11456. https://doi.org/10.1021/acs.chemrev.8b00422.

3. Chen, J., Fan, X., Li, Q., Yang, H., Khoshi, M.R., Xu, Y., Hwang, S., Chen, L., Ji, X., Yang, C., et al. (2020). Electrolyte design for LiF-rich solid–electrolyte interfaces to enable high-performance microsized alloy anodes for batteries. Nat. Energy *5*, 386–397. https://doi.org/10.1038/s41560-020-0601-1.

4. Recham, N., Chotard, J.N., Dupont, L., Delacourt, C., Walker, W., Armand, M., and Tarascon, J.-M. (2010). A 3.6 V lithium-based fluorosulphate insertion positive electrode for lithium-ion batteries. Nat. Mater. *9*, 68–74. https://doi.org/10.1038/nmat2590.

5. Okubo, M., Ko, S., Dwibedi, D., and Yamada, A. (2021). Designing positive electrodes with high energy density for lithium-ion batteries. J. Mater. Chem. A *9*, 7407–7421. https://doi.org/10.1039/D0TA10252K.

6. Campbell, G.A. (2020). The cobalt market revisited. Miner. Econ. *33*, 21–28. https://doi.org/10.1007/s13563-019-00173-8.

7. Henze, V. (2021). Battery pack prices fall to an average of $132/kWh, but rising commodity prices start to bite. BloombergNEF. https://about.bnef.com/blog/battery-pack-prices-fall-to-an-average-of-132-kwh-but-rising-commodity-prices-start-to-bite/.

8. Su, D., Zhou, D., Wang, C., and Wang, G. (2018). Toward high performance lithium–sulfur batteries based on Li$_2$S cathodes and beyond: status, challenges, and perspectives. Adv. Funct. Mater. *28*, 1800154. https://doi.org/10.1002/adfm.201800154.

9. Luo, S., Wu, F., and Yushin, G. (2021). Strategies for fabrication, confinement and performance boost of Li$_2$S in lithium-sulfur, silicon-sulfur &

CellPress

Joule
Article

related batteries. Mater. Today 49, 253–270. https://doi.org/10.1016/j.mattod.2021.03.017.

10. Chase, M.W.; NIST (1998). NIST-JANAF thermochemical tables (American Chemical Society)9. https://doi.org/10.18434/T42S31.

11. Holmes, C.F. (1986). Lithium/halogen batteries. In Batteries Implantable Biomed. Devices (Springer), pp. 133–180. https://doi.org/10.1007/978-1-4684-9045-9_6.

12. Zhu, G., Tian, X., Tai, H.-C., Li, Y.-Y., Li, J., Sun, H., Liang, P., Angell, M., Huang, C.-L., Ku, C.-S., et al. (2021). Rechargeable Na/Cl₂ and Li/Cl₂ batteries. Nature 596, 525–530. https://doi.org/10.1038/s41586-021-03757-z.

13. Li, X., Wang, Y., Chen, Z., Li, P., Liang, G., Huang, Z., Yang, Q., Chen, A., Cui, H., Dong, B., et al. (2022). Two-electron redox chemistry enabled high-performance iodide-ion conversion battery. Angew. Chem. 61. e202113576. https://doi.org/10.1002/anie.202113576.

14. Guo, Q., Kim, K.-I., Li, S., Scida, A.M., Yu, P., Sandstrom, S.K., Zhang, L., Sun, S., Jiang, H., Ni, Q., et al. (2021). Reversible insertion of I–Cl interhalogen in a graphite cathode for aqueous dual-ion batteries. ACS Energy Lett. 6, 459–467. https://doi.org/10.1021/acsenergylett.0c02575.

15. Yang, C., Chen, J., Ji, X., Pollard, T.P., Lü, X., Sun, C.-J., Hou, S., Liu, Q., Liu, C., Qing, T., et al. (2019). Aqueous Li-ion battery enabled by halogen conversion–intercalation chemistry in graphite. Nature 569, 245–250. https://doi.org/10.1038/s41586-019-1175-6.

16. Bryantsev, V.S., Giordani, V., Walker, W., Blanco, M., Zecevic, S., Sasaki, K., Uddin, J., Addison, D., and Chase, G.V. (2011). Predicting solvent stability in aprotic electrolyte Li–air batteries: nucleophilic substitution by the superoxide anion radical (O2●⁻). J. Phys. Chem. A 115, 12399–12409. https://doi.org/10.1021/jp2073914.

17. Schwenke, K.U., Meini, S., Wu, X., Gasteiger, H.A., and Piana, M. (2013). Stability of superoxide radicals in glyme solvents for non-aqueous Li–O₂ battery electrolytes. Phys. Chem. Chem. Phys. 15, 11830–11839. https://doi.org/10.1039/C3CP51531A.

18. Yoshida, K., Nakamura, M., Kazue, Y., Tachikawa, N., Tsuzuki, S., Seki, S., Dokko, K., and Watanabe, M. (2011). Oxidative-stability enhancement and charge transport mechanism in glyme–lithium salt equimolar complexes. J. Am. Chem. Soc. 133, 13121–13129. https://doi.org/10.1021/ja203983r.

19. Jiao, S., Ren, X., Cao, R., Engelhard, M.H., Liu, Y., Hu, D., Mei, D., Zheng, J., Zhao, W., Li, Q., et al. (2018). Stable cycling of high-voltage lithium metal batteries in ether electrolytes. Nat. Energy 3, 739–746. https://doi.org/10.1038/s41560-018-0199-8.

20. Ren, X., Zou, L., Cao, X., Engelhard, M.H., Liu, W., Burton, S.D., Lee, H., Niu, C., Matthews, B.E., Zhu, Z., et al. (2019). Enabling high-voltage lithium-metal batteries under practical conditions. Joule 3, 1662–1676. https://doi.org/10.1016/j.joule.2019.05.006.

21. Zhang, J., Wang, P.F., Bai, P., Wan, H., Liu, S., Hou, S., Pu, X., Xia, J., Zhang, W., Wang, Z., et al. (2021). Interfacial design for a 4.6 V high-voltage single-crystalline LiCoO₂ cathode. Adv. Mater. 34, 2108353. https://doi.org/10.1002/adma.202108353.

22. Choudhury, S., Tu, Z., Nijamudheen, A., Zachman, M.J., Stalin, S., Deng, Y., Zhao, Q., Vu, D., Kourkoutis, L.F., Mendoza-Cortes, J.L., and Archer, L.A. (2019). Stabilizing polymer electrolytes in high-voltage lithium batteries. Nat. Commun. 10, 3091. https://doi.org/10.1038/s41467-019-11015-0.

23. Weber, R., Genovese, M., Louli, A.J., Hames, S., Martin, C., Hill, I.G., and Dahn, J.R. (2019). Long cycle life and dendrite-free lithium morphology in anode-free lithium pouch cells enabled by a dual-salt liquid electrolyte. Nat. Energy 4, 683–689. https://doi.org/10.1038/s41560-019-0428-9.

24. Mao, M., Huang, B., Li, Q., Wang, C., He, Y.-B., and Kang, F. (2020). In-situ construction of hierarchical cathode electrolyte interphase for high performance LiNi₀.₈Co₀.₁Mn₀.₁O₂/Li metal battery. Nano Energy 78, 105282. https://doi.org/10.1016/j.nanoen.2020.105282.

25. Hérold, A. (1987). Synthesis of graphite intercalation compounds. In Chemical Physics of Intercalation, pp. 3–45. https://doi.org/10.1007/978-1-4757-9649-0_1.

26. Muhuri, P.K., Das, B., and Hazra, D.K. (1997). Ionic association of some lithium salts in 1,2-dimethoxyethane. A Raman spectroscopic and conductivity study. J. Phys. Chem. B 101, 3329–3332. https://doi.org/10.1021/jp963747d.

27. Fisher, L.R., and Israelachvili, J.N. (1979). Direct experimental verification of the Kelvin equation for capillary condensation. Nature 277, 548–549. https://doi.org/10.1038/277548a0.

28. Mayer, U., Gutmann, V., and Gerger, W. (1975). The acceptor number—a quantitative empirical parameter for the electrophilic properties of solvents. Monatshefte für Chemie/Chemical Monthly 106, 1235–1257. https://doi.org/10.1007/BF00913599.

29. Henderson, W.A., Brooks, N.R., Brennessel, W.W., and Young, V.G. (2003). Triglyme−Li⁺ cation solvate structures: models for amorphous concentrated liquid and polymer electrolytes (I). Chem. Mater. 15, 4679–4684. https://doi.org/10.1021/cm034351z.

30. Henderson, W.A., Brooks, N.R., and Young, V.G. (2003). Tetraglyme−Li⁺ cation solvate structures: models for amorphous concentrated liquid and polymer electrolytes (II). Chem. Mater. 15, 4685–4690. https://doi.org/10.1021/cm034352r.

31. Abraham, K.M., and Alamgir, M. (1987). Spectroscopic and electrochemical studies on some halogens and interhalogens in SOCl₂. J. Electrochem. Soc. 134, 2112–2118.

32. Shkrob, I.A., Zhu, Y., Marin, T.W., and Abraham, D.P. (2013). Mechanistic Insight into the protective action of bis(oxalato)borate and difluoro(oxalate)borate anions in Li-Ion Batteries. J. Phys. Chem. C 117, 23750–23756. https://doi.org/10.1021/jp407714p.

33. Qiu, X., Thompson, J.W., and Billinge, S.J.L. (2004). PDFgetX2: a GUI-driven program to obtain the pair distribution function from X-ray powder diffraction data. J. Appl. Crystallogr. 37, 678. https://doi.org/10.1107/S0021889804011744.

34. Huang, W., Frech, R., and Wheeler, R.A. (1994). Molecular structures and normal vibrations of trifluoromethane sulfonate (CF₃SO₃⁻) and its lithium ion pairs and aggregates. J. Phys. Chem. 98, 100–110. https://doi.org/10.1021/j100052a018.

35. Han, S.-D., Allen, J.L., Jónsson, E., Johansson, P., McOwen, D.W., Boyle, P.D., and Henderson, W.A. (2013). Solvate structures and computational/spectroscopic characterization of lithium difluoro(oxalato)borate (LiDFOB) electrolytes. J. Phys. Chem. C 117, 5521–5531. https://doi.org/10.1021/jp309102c.

36. Rosenman, A., Elazari, R., Salitra, G., Markevich, E., Aurbach, D., and Garsuch, A. (2015). The effect of interactions and reduction products of LiNO₃, the anti-shuttle agent, in Li-S battery systems. J. Electrochem. Soc. 162, A470–A473. https://doi.org/10.1149/2.0861503jes.

37. Tian, H., Gao, T., Li, X., Wang, X., Luo, C., Fan, X., Yang, C., Suo, L., Ma, Z., Han, W., and Wang, C. (2017). High power rechargeable magnesium/iodine battery chemistry. Nat. Commun. 8, 14083. https://doi.org/10.1038/ncomms14083.

38. Cui, C., Yang, C., Eidson, N., Chen, J., Han, F., Chen, L., Luo, C., Wang, P.F., Fan, X., and Wang, C. (2020). A highly reversible, dendrite-free lithium metal anode enabled by a lithium-fluoride-enriched interphase. Adv. Mater. 32. e1906427. https://doi.org/10.1002/adma.201906427.

39. Hooley, J.G., and Smee, J.L. (1964). The mechanism of the bromination of graphite. Carbon 2, 135–138. https://doi.org/10.1016/0008-6223(64)90054-5.

40. Selig, H., and Ebert, L.B. (1980). Graphite intercalation compounds. Adv. Inorg. Chem. Radiochem. 23, 281–327. https://doi.org/10.1016/S0065-2792(08)60095-3.

41. Zhao, Q., Lu, Y., Zhu, Z., Tao, Z., and Chen, J. (2015). Rechargeable lithium-iodine batteries with iodine/nanoporous carbon cathode. Nano Lett. 15, 5982–5987. https://doi.org/10.1021/acs.nanolett.5b02116.

42. Zhao, X., Zhao-Karger, Z., Fichtner, M., and Shen, X. (2020). Halide-based materials and chemistry for rechargeable batteries. Angew. Chem. Int. Ed. Engl. 59, 5902–5949. https://doi.org/10.1002/anie.201902842.

43. Kasrai, M., Fleet, M.E., Bancroft, G.M., Tan, K.H., and Chen, J.M. (1991). X-ray-absorption near-edge structure of alkali halides: the interatomic-distance correlation. Phys. Rev. B Condens. Matter 43, 1763–1772. https://doi.org/10.1103/PhysRevB.43.1763.

44. Pacilé, D., Meyer, J.C., Fraile Rodríguez, A.F., Papagno, M., Gómez-Navarro, C., Sundaram, R.S., Burghard, M., Kern, K., Carbone, C., and Kaiser, U. (2011). Electronic properties and atomic structure of graphene oxide membranes. Carbon 49, 966–972. https://doi.org/10.1016/j.carbon.2010.09.063.

45. Sun, T., Sun, G., Yu, F., Mao, Y., Tai, R., Zhang, X., Shao, G., Wang, Z., Wang, J., and Zhou, J. (2021). Soft X-ray ptychography chemical imaging of degradation in a composite surface-reconstructed Li-rich cathode. ACS Nano 15, 1475–1485. https://doi.org/10.1021/acsnano.0c08891.